IMPROVEMENT OF THE PERFORMANCE OF SMALL-SIZED CAVITATING VENTURIS BY INSERTING OBSTACLES

by

Brahim ROSTANE[a], Khaled ALIANE[a], Mohammed BRAYYICH[b], Sajad A. ZEARAH[c], Ali AKGUL[d,e*], Barno ABDULLAEVA[f], Younes MENNI[g], Abdulrhman M. ALSHARARI[h], and Jihad ASAD [i]

[a] Computational Mechanics Research laboratory (MECACOMP), Faculty of Technology, University Abou Bekr Belkaid, Tlemcen, Algeria
[b] College of Engineering, National University of Science and Technology, Dhi Qar, Iraq
[c] Scientific Research Center, Al-Ayen University, Thi-Qar, Iraq
[d] Department of Mathematics, Art and Science Faculty, Siirt University, Siirt, Turkey
[e] Department of Electronics and Communication Engineering, Saveetha School of Engineering, SIMATS, Chennai, Tamilnadu, India
[f] Tashkent State Pedagogical University named after Nizami, Tashkent, Uzbekistan
[g] Department of Technology, University Center Salhi Ahmed Naama (Ctr. Univ. Naama), Naama, Algeria
[h] Department of Physics, University of Tabuk, Tabuk, Saudi Arabia
[i] Department of Physics, Faculty of Applied Science, Palestine Technical University – Kadoorie, Tulkarm, Palestine

Original scientific paper
https://doi.org/10.2298/TSCI2304467R

Cavitating Venturis are simple apparatus used as a flow meter over a broad range of mass-flow rates. The main objective of this work is to introduce obstacles in small-sized cavitating Venturis in order to increase their capacity by raising the critical pressure, i.e. widens the phase of the cavitating mode. Four configurations have been tested depending on the location of these obstacles. This study focused on investigating the numerical performance of cavitating Venturis with different downstream pressures by employing the k-ω SST turbulence model and the Rayleigh-Plesset equation for modeling cavitation. The governing equations were solved using the finite volume method, employing the Rhie and Chow pressure-velocity coupling scheme. The results showed the void fraction and streamlines contours obtained on the symmetry plane. The mass-flow ratio was presented for all configurations and different pressure ratios. The study showed that the cavitating Venturis equipped with obstacles extend the phase of choked mode from 10.71% to 21.42% and that the best configuration correspond to the case where the obstacles are placed in the converging section.

Key words: *cavi tating Venturis, flow meter, two-phase flow, ANSYS-CFX*

Introduction

Cavitation is a process of vapor bubbles formation in a fluid-flow because of the pressure reduction below the vaporization pressure. This decrease in pressure occurs through the reduction in cross-section in a confined flow, usually in the throat of the Venturi. Cavitating Venturis are convergent-divergent geometries used to measure mass-flow rate with high accuracy

* Corresponding author, e-mail: aliakgul@siirt.edu.tr

and can be used as control devices [1]. They are beneficial in devices that need a steady flow of liquid at a very low mass-flow rate. Since the 1960's, several researchers have examined through both experimental and numerical means the performance of cavitating Venturis by measuring and evaluating the mass-flow rates and pressure loses. For example, see Xu *et al.* [2] and Ulas [3]. Dastane *et al.* [4] developed a single-phase and multi-phase approach for modeling cavitation flows in a Venturi tube using the Singhal cavitation model. Dittakavi *et al.* [5] carried out a large scale simulation of turbulent cavitating flow. They found that, due to turbulence, vapor formation at the Venturi throat suppresses velocity fluctuations. Decaix and Goncalves [6] used a new scale-adaptive model and a detached eddy simulation to conduct an unsteady numerical study of the behavior of a cavitation region developed across a Venturi pattern. Experimental data was compared to both 2-D and 3-D simulations. In their experiment, Tian *et al.* [7] investigated the effectiveness of a cavitating Venturi. They achieved this by placing a controllable pintle in the throat of the Venturi, which was located concentrically. The authors examined the mass-flow rate under different coupling positions. An experimental study was conducted by Bermejo *et al.* [8] to evaluate the dynamic performance of a fluid-flow in the cavitating Venturi. With and without cavitation, fluid-flows were created for the experiment, ultimately revealing that the inlet pressure of the Venturi impacts the effectiveness of cavitation flows. Ashrafizadeh and Ghassemi [9] studied, experimentally and numerically, small-size cavitating Venturis for mass-flow rate regulation. Geometric parameters and upstream and downstream pressures were among the factors that the researchers scrutinized when exploring how the mass-flow rate is affected. Proper orthogonal decomposition and dynamic mode decomposition were introduced by Yadong and Lei [10] and Han *et al.* [11] to examine the coherent structures of cavitation and flow fields in three dimensions. The authors discovered that the dynamic decomposition mode can precisely catch the way the flow works and its most significant dynamic behavior in cavitational flow. The application of obstacles is primarily to control the fluid-flow and improve the heat transfer in the channel, see Rostane *et al.* [12] and Rostane and Abboudi [13]. This method is also considered to be a potential way to control the flow behavior and associated unstable cavitational phenomena occurring in a pump. Many of researchers re-examined experimentally or numerically the mechanism of cloud cavitation and the impact of obstacles on cavity shapes, noise issuance, lift and drag vacillations and resistance of the cavity, see Kawanami *et al*. [14], Pham *et al.* [15], Sato and Saito [16], Zhao *et al.* [17], Che *et al.* [18], and Zhang *et al.* [19]. Their findings contributed to the improvement of the geometric arrangement of obstacles present within the pump. Additionally, to prevent re-entrant jets, obstacle-triggered pressure oscillations had also been shown to be physically beneficial in suppressing cavitation. Recently, Zhao *et al.* [20] established a research that combined numerical analysis with experimental of the cavitation flow to investigate the passive control of the cavitation by the obstacles of the blades in an inlet guide vane water jet pump. Their results indicated that the cavities were almost disappeared at the leading edge of the blades before the obstacle whereas the shear cavitation is triggered after each obstacle. Therefore, this phenomenon avoided the impact of the dynamic load around the leading edge regimes and thus it allowed mitigating the damage due to the erosion of materials.

As seen previously, cavitating Venturis have various applications as a flow meter for measuring mass-flow rate across a broad range. The flow within the Venturi will be throttled if the critical pressure ratio, which measures downstream and upstream pressure ratio, is less than 0.8. As a result, the mass-flow rate will remain constant. Thus, to measure it, we just need to know the upstream pressure. Therefore, to enhance the flow-meter capacity, it is necessary to increase the critical pressure ratio. Consequently, it is required to find a way to in-

crease the intensity of the cavitation. In order to ensure this, the cavitation can be controlled using obstacles. Therefore, the primary aim of this work is to introduce obstacles in small-sized cavitating Venturis, in order to increase the critical pressure. Numerical analysis has been conducted in this study to examine the effectiveness of cavitating Venturis.

Basic equations and computational methods

In this research, four configurations have been studied:

- *1st configuration.* Figure 1(a) illustrates a schematic representation of the Venturi configurations and highlighting its main dimensions. This configuration has been analyzed through experimental and numerical investigations that were published by Ashrafizadeh and Ghassemi [9]. The diameter and length of the throat are both 1 mm. The converging angle is fixed at 15° while that of the diverging one is 7°. The diameter of inlet and outlet sections is equal to 4 mm.
- *2nd configuration.* Figure 1(b) presents the same previous configuration with the insertion of 6 cubic obstacles of 0.2 mm in height placed on the symmetry plane of the converging section.
- *3rd configuration*. Figure 1(c) presents the first configuration with the insertion of six obstacles placed on the symmetry plane of the diverging section.
- *4th configuration.* Figure 1(d) presents the two previous configurations together (twelve obstacles placed in the converging and diverging sections).

The positions of these obstacles and the distances between them are given in fig. 1(e).

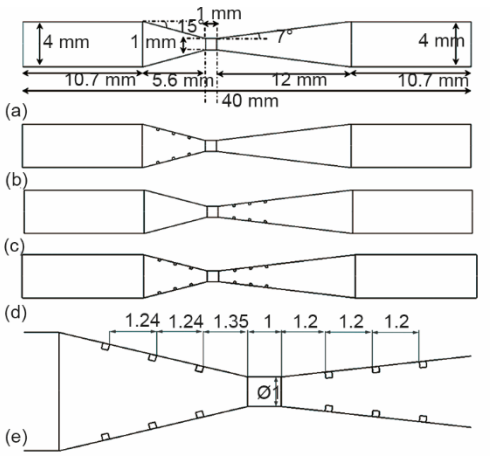

Figure 1. Description of the studied Venturis; (a) 1st configuration, (b) 2nd configuration, (c) 3rd configuration, (d) 4th configuration, and (e) distances between obstacles

The continuity and momentum equations employing the mixture multiphase approach are the governing equations for the two-phase flow in the Venturi. The continuity equation for the mixture is:

$$\frac{\partial}{\partial_t}(\rho_{\mathrm{m}}) + \nabla(\rho_{\mathrm{m}} U_{\mathrm{m}}) = 0 \tag{1}$$

The velocity of the mixture is expressed by:

$$U_{\mathrm{m}} = \frac{\sum_{n=1}^{2} \alpha_n \rho_n \mathrm{U}_n}{\rho_{\mathrm{m}}} \tag{2}$$

The density of the mixture is expressed as:

$$\rho_{\mathrm{m}} = \sum_{n=1}^{2} \alpha_n \rho_n \tag{3}$$

where α represents the volume fraction, while n denotes the number of phases. The momentum equation for the mixture can be given as:

$$\frac{\partial}{\partial_t}(\rho_{\mathrm{m}}U_{\mathrm{m}}) + \nabla(\rho_{\mathrm{m}}U_{\mathrm{m}}U_{\mathrm{m}}) = -\nabla p + \nabla\mu[\nabla U_{\mathrm{m}} + (\nabla U_{\mathrm{m}})^T] \tag{4}$$

with

$$\mu = \mu_{\mathrm{m}} + \mu_t \text{ and } \mu_{\mathrm{m}} = \sum_{n=1}^{2}\alpha_n\mu_n \tag{5}$$

The momentum equation contains the Reynolds stress terms when the flow is turbulent. These stresses were modeled using the shear stress transport model *k-ω* SST. Menter's *k-ω* SST model [21] produces very accurate forecasts of the onset and magnitude of the flow separation [22]. It is robust and still economical [4, 23, 24]. For modeling cavitation, ANSYS CFX 16 uses the Rayleigh-Plesset equation which defines the expansion and the collapse of a vapor bubble exposed to a pressure disruption. This model has been adjusted to model both vaporization and condensation phases of cavitation. The Rayleigh-Plesset equation can be expressed:

$$R_{\mathrm{B}}\frac{\mathrm{d}^2R_{\mathrm{B}}}{\mathrm{d}t^2} + \frac{3}{2}\left(\frac{\mathrm{d}R_{\mathrm{B}}}{\mathrm{d}t}\right)^2 + \frac{2\sigma}{\rho_f R_{\mathrm{B}}} = \frac{p_{\mathrm{v}} - p}{\rho_f} \tag{6}$$

where σ represents the surface tension coefficient, R_{B} – the bubble radius, p_{v} – the vapor pressure, ρ_f – the liquid density, and p – the pressure in the fluid enclosing the bubble. The final expression of the total interphase mass transfer rate per volume unit is given by the following forms:

If $p < p_{\mathrm{v}}$:

$$\dot{m}_{fv} = F_{\mathrm{vap}}\frac{3\alpha_{\mathrm{nuc}}\ (1-\alpha)\rho_v}{R_{\mathrm{nuc}}}\sqrt{\frac{2}{3}\frac{|p_{\mathrm{v}} - p|}{\rho_f}}\mathrm{sign}\left(p_{\mathrm{v}} - p\right) \tag{7}$$

If $p > p_{\mathrm{v}}$:

$$\dot{m}_{fv} = F_{\mathrm{cond}}\frac{3\alpha\,\rho_{\mathrm{v}}}{R_{\mathrm{B}}}\sqrt{\frac{2}{3}\frac{|p_{\mathrm{v}} - p|}{\rho_f}}\mathrm{sign}\left(p_{\mathrm{v}} - p\right) \tag{8}$$

where R_{nuc} is a nucleation site radius and α_{nu} is the nucleation site fractional volume. The subsequent parameters are used in the Rayleigh-Plesset cavitation model that was introduced in ANSYS CFX: $F_{\mathrm{cond}} = 0.01$, $F_{\mathrm{vap}} = 50$, $R_{\mathrm{B}} = 10^{-6}\,m$, and $\alpha_{\mathrm{nuc}} = 5 \times 10^{-4}$.

The 3-D studies of these cases were employed using ANSYS CFX 16. The fluid used was the water at 27 °C. The flow boundary conditions were determined according to inlet and outlet pressure. The inlet pressure was kept constant at 20 bar whereas the outlet pressure values were variable. No-slip conditions were applied at the solid walls (Venturi, cubes). The instructed meshes were employed to solve the previously equations cited in steady-state conditions. These structures were refined near the solid walls and throat region where there was two-phase flow. The finite volume method was used to solve continuity and momentum equations. The convection term was solved using the second order upwind scheme and the Rhie and Chow approach [25] was employed to resolve the pressure-velocity coupling. The solution was considered convergent when the residue was less than 10^{-6}.

Results and discussions

The amount of the mesh has a significant impact on the precision of the seeking solution in any numerical study. Mesh sensitivity tests are therefore necessary to ensure a solution regardless of the selected calculation grid. The current investigation utilized four meshes

of 611234, 925878, 1261544, and 1515462 cells were tested for the case of an inlet pressure of 20 bar and a downstream pressure fixed at 12 bar. The results obtained, using the four grids, were compared quantitatively by considering the numerical uncertainties to predict the mass-flow, $\dot{m}_{\text{liq}}$, described as the measured mass-flow rate of the liquid at the outlet of the Venturi. The error gap between values of the ratios of the mass-flow obtained using grids 3 and 4 was equal to 0.085%. Therefore, it is considered that the solution remains not dependent by the mesh when passing from a grid of 1261544 to another of 1515462. The relative error, δ, indicated in tab. 1, is calculated by the following relation:

$$\delta = \left| \frac{\dot{m}_{\text{liq},i} - \dot{m}_{\text{liq},i+1}}{\dot{m}_{\text{liq},i}} \right| 100 \tag{9}$$

Table 1. Mesh sensitivity test

Grid	Cell number	M_{liq} [kgs^{-1}]	δ [%]
1	611234	0.0460251	0.611
2	925878	0.0463064	0.249
3	1261544	0.0464196	0.085
4	1515462	0.0464521	–

As noted previously, there are two operating modes in the cavitating Venturi. The first mode is the choked mode where cavitation takes place in the throat. Thus, the fluid-flow comes to be choked. In this state, the mass-flow rate stays the same and does not depend on the downstream pressure, fig. 2. A two-phase flow is created at the throat and diffuser section under these conditions. In the diffuser section, the vapor zone ends with the reattachment of the liquid flow to this area.

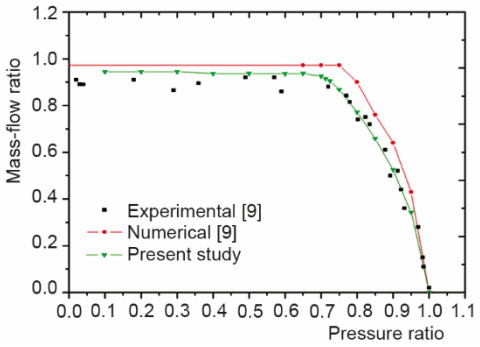

Figure 2. Proof of validity by comparison with others [9]

An increase in the downstream pressure implies a shifting of the reattachment point towards direction of the throat [1, 9]. The second mode is the all-liquid mode where cavitation cannot occur. This mode occurs when a critical level of downstream pressure is achieved where the liquid flow gets at the throat. Then, as downstream pressure rises, the mass-flow rate declines, fig. 2.

In both modes, the mass-flow ratio, $\dot{m}_{\text{r}}$, defined as the proportion of the liquid's measured mass-flow rate at the Venturi outflow, $\dot{m}_{\text{liq}}$, to the choked mass-flow rate, $\dot{m}_{\text{choked}}$, being expressed by:

$$\dot{m}_{\text{r}} = \frac{\dot{m}_{\text{liq}}}{\dot{m}_{\text{choked}}} \tag{10}$$

$$\dot{m}_{\text{choked}} = A_{th}\sqrt{2\rho(P_{\text{in}} - P_{\text{sat}})} \tag{11}$$

The pressure ratio P_r can also be used to indicate the downstream pressure of the Venturi in a dimensionless format:

$$P_r = \frac{P_{out} - P_{sat}}{P_{in} - P_{sat}}$$

The following formula is used to calculate the critical pressure ratio $P_{r,crit}$ at the junction of the choked flow and the all-liquid flow regions [9]:

$$P_{r,crit} = 1 - K_l \tag{12}$$

where K_l is the pressure drop coefficient across the Venturi under conditions of all liquid. In fig. 2, experimental and numerical data from the work of Ashrafizadeh and Ghassemi [9] were compared with our numerical results for the Venturi. They expressed the evolution of the mass-flow ratio, $\dot{m}_r$, *vs.* the pressure ratio. P_r, described as the ratio of the pressure at the outlet to that at the inlet of the cavitating Venturi. As can be observed, the cavitating Venturis (CV) is capable of maintaining a constant mass-flow rate until a critical pressure ratio $P_{r,crit}$ from which the mass-flow ratio drops rapidly. Our numerical findings match the experimental data very well. They are closer compared to those of Ashrafizadeh and Ghassemi [9]. The experimental data have a critical pressure ratio of about 0.72, whereas the simulated results have a critical pressure ratio of about 0.70. So, the results are very satisfactory.

Concerning the streamlines, fig. 3, there is the emergence of a recirculation zone or a secondary vortex flow at the diverging section due to the flow separation at the wall. This phenomenon is caused by the adverse pressure gradient in this place. This zone has also been identified in the work of Ashrafizadeh and Ghassemi [9].

Figure 4 depicts the change in $\dot{m}_r$ as a function of P_r. In this figure, all the curves indicate two phases: the first phase is the cavitation phase where the mass-flow rate stays unchanged (throttled mode) while the second represent the all-liquid state, in which the relationship between the mass-flow rate and outlet pressure is inverse. By comparing the four configurations, tab. 2, the cavitating Venturis equipped with obstacles placed in the converging section has a critical pressure: $P_{r,crit}$ = 0.85. Therefore, the throttled mode has been enlarged by 21.42% compared to the cavitating Venturis without obstacles. The other two configurations, cavitating Venturis equipped with obstacles at the diffuser and cavitating Venturis with obstacles placed in the converging and diverging sections, have the same form where their critical pressure is equal to 0.775 with a throttled mode widening of 10.71%. In the two-phase vapor-liquid flows, the void fraction is interpreted as the volume fraction occupied by the vapor phase. Therefore, the void fraction contours show clearly the cavitation region from its appearance until its dissipation.

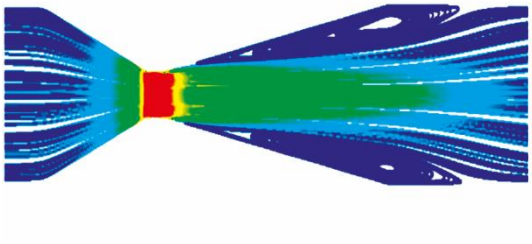

Figure 3. Streamlines on the symmetry plane

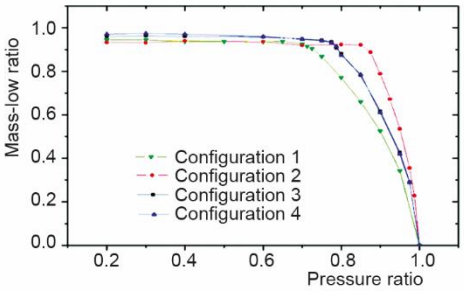

Figure 4. Variation of the mass-flow ratio *vs.* the pressure ratio

Table 2. Chocked mode extension

	1st case	2nd case	3rd case	4th case
$P_{r,crit}$	0.72	0.85	0.775	0.775
Chocked mode extension	_	21.42%	10.71%.	10.71%.

Figures 5(a)-5(d) show the development of the void fraction in relation to downstream pressure with an upstream pressure set at 20 bar. It is clear that the cavitation region is larger for low outlet pressures. However, by raising the downstream pressure, the cavitation region is limited near the solid wall of diverging section, very close to the throat until it had disappeared. This phenomenon was widely discussed in the study conducted by Ashrafizadeh and Ghassemi [9]. Comparing the different cases, fig. 5, it turns out that the void fraction is greater for the cavitating Venturis cases with obstacles placed in converging part, 2nd case. This is in agreement with fig. 4 where the $P_{r,crit}$ is the largest for this case.

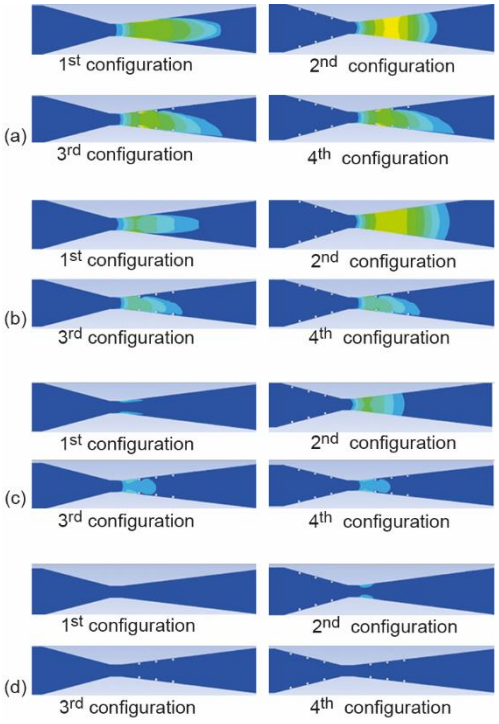

Figure 5. Contours of the void fraction in the studied Venturis for P_{in} = 20 bar; (a) P_{out} = 4 bar, (b) P_{out} = 8 bar, (c) P_{out} = 12 bar, and (d) P_{out} = 16 bar

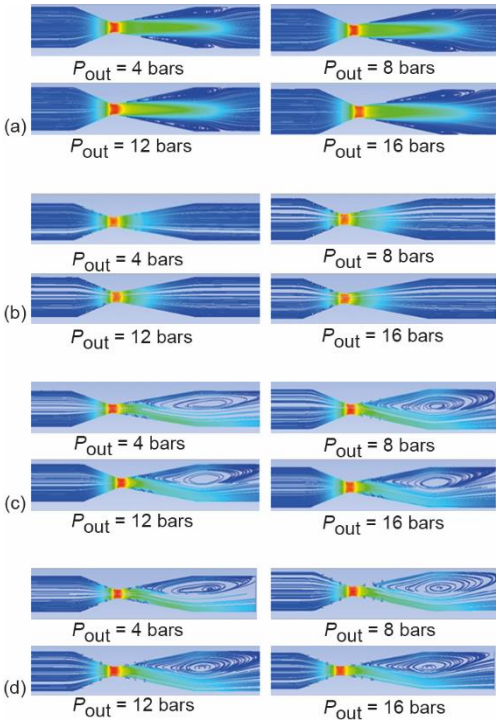

Figure 6. Streamlines on the symmetry plane for the four configurations with different outlet pressures; (a) 1st configuration, (b) 2nd configuration, (c) 3rd configuration, and (d) 4th configuration

This phenomenon is clearly seen in the figures of the P_{out} equal to 8 bar, fig. 5(b) and 12 bar, fig. 5(c), where the vapor phase remains present even at the downstream pressure of 16 bar, fig. 5(d). Figure 6 shows the streamlines for the different cases studied and for the outlet pressures: 5 bar, 10 bar, 12 bar, and 16 bar. For cavitating Venturis without obstacle (configura-

tion 1), the appearance of a recirculation zone or a vortex secondary flow could be seen near the diverging wall due to the fluid-flow separation from the solid wall. With regard to configurations 3 and 4, a vortex zone is observed at the upper wall of the diverging part. On the other hand, for the second case where the obstacles are placed in the converging section, the recirculation zone disappears completely. The obstacles placed in the diverging section in tandem position disturb the recirculation zones by increasing the diffusion of vorticities. Consequently, the volume of one of the vortices increases and takes the upper half of this section.

Then, the flow will necessarily force a passage by sinking downwards. For the cubes placed before the separation points, their positions allow elimination of the recirculation zones. This phenomenon can be explained as follows. The obstacles placed in the converging section, which was upstream of the separation region, allow energy to be brought locally at the boundary layer near the wall so as to divert the flow separation. These obstacles locally produce vortices which reinforce momentum transfers in the middle of the boundary layer. Therefore, the amount of motion subtracted in the part which is far from the wall, in which the velocities are high, is brought by the vortex towards the wall (where the velocities are low because of the friction at the wall). This transfer of momentum allows the boundary layer to counteract for longer the unfavorable longitudinal pressure gradient responsible for the boundary layer detachment. This technique has been well demonstrated in aerodynamic studies and has been the subject of several patents [26, 27].

Consequently, the appearance of obstacles contributes to the reduction of vortex zone which is in the diverging section. Thus, hydraulic losses will be reduced according to eq. (12), $P_{r,crit}$ is inversely proportional to the pressure drop coefficient K_l. Therefore, the critical P ratio increases.

Conclusions

In this study, the obstacle insertion effect in the small-sized cavitating Venturi and their influence on the operating parameters of the latter were investigated numerically. Four configurations have been chosen where the obstacles are placed either in converging, diverging or both sections at the same time. The cavitation zone is wider for low outlet pressures. However, by raising the downstream pressure, the cavitation region is limited near the solid wall of diverging section, very close to the throat until it disappears. The cavitating Venturis equipped with obstacles placed in converging section has a critical pressure ratio equal to 0.85. Therefore, the chocked mode has been enlarged by 21.42% compared to cavitating Venturis without obstacles. For the cases of cavitating Venturis equipped with obstacles in diverging part and cavitating Venturis with obstacles placed in converging and diverging sections, they have a critical pressure ratio equal to 0.775 with a throttled mode widening of 10.71%. Addition of obstacles contributes to the reduction of the pressure drops in diverging section of cavitating Venturi. It implies that the region of the cavitating Venturis in choked mode (cavitating mode) assumes greater significance. Due to the fact that cavitating Venturis are built to function in their choked mode, this phenomena is quite advantageous.

References

[1] Ghassemi, H., Fasih, H. F., Application of Small Size Cavitating Venturi As Flow Controller and Flow Meter, *Flow Measurement and Instrumentation*, *22* (2011), 5, pp. 406-412
[2] Xu, C., *et al.*, Modeling Cavitating Venturi Flows, *Journal of Propulsion and Power*, *18* (2002), 6, pp. 1227-1234
[3] Ulas, A., Passive Flow Control in Liquid-Propellant Rocket Engines with Cavitating Venturi, *Flow Measurement and Instrumentation*, *17* (2006), 2, pp. 93-97

[4] Dastane, G. G., *et al.*, Single and Multiphase CFD Simulations for Designing Cavitating Venturi, *Chemical Engineering Research and Design*, *149* (2019), Sept., pp. 1-12
[5] Dittakavi, N., *et al.*, Large Eddy Simulation of Turbulent-Cavitation Interactions in a Venturi Nozzle, *Journal of Fluids Engineering*, *132* (2010), 12, 121301
[6] Decaix, J., Goncalves, E., Investigation of Three-Dimensional Effects on a Cavitating Venturi Flow, *International Journal of Heat and Fluid-flow*, *44* (2013), Dec., pp. 576-595
[7] Tian, H., *et al.*, Application of Variable Area Cavitating Venturi as a Dynamic Flow Controller, *Flow Measurement and Instrumentation*, *38* (2014), Aug., pp. 21-26
[8] Bermejo, D., *et al.*, Experimental Investigation of a Cavitating Venturi and Its Application to Flow Metering, *Flow Measurement and Instrumentation*, *78* (2021), Apr., 101868
[9] Ashrafizadeh, S. M., Ghassemi, H., Experimental and Numerical Investigation on the Performance of Small-Sized Cavitating Venturis, *Flow measurement and Instrumentation*, *42* (2015), Apr., pp. 6-15
[10] Han, Y. D., Tan, L., Experimental Study of Venturi Cavitation Flow and Kinetic Modal Decomposition, *J. Mech. Eng*, *55* (2019), 18, pp. 173-179
[11] Han, Y., *et al.*, Method of Data-Driven Mode Decomposition for Cavitating flow in a Venturi Nozzle, *Ocean Engineering*, *261* (2022), Oct., 112114
[12] Rostane, B., *et al.*, Three Dimensional Simulation for Turbulent Flow Around Prismatic Obstacle with Rounded Downstream Edge Using the *k-ω* SST Model, *International Review of Mechanical Engineering (I. RE. ME)*, *9* (2015), 3, pp. 1970-8734
[13] Rostane, B., Abboudi, S., Numerical Study of Laminar Fluid-flow Around Two Heated Wall-Mounted Perforated Cubes in Tandem Arrangement, *IJHT, 40* (2022), 1, pp. 157-166
[14] Kawanami, Y., *et al.*, Mechanism and Control of Cloud Cavitation, *Journal of Fluids Engineering*, *119* (1997), 4, pp. 788-794
[15] Pham, T. M., *et al.*, Investigation of Unsteady Sheet Cavitation and Cloud Cavitation Mechanisms, *Journal of Fluids Engineering*, *121* (1999), 2, pp. 289-296
[16] Sato, K., Saito, Y., Unstable Cavitation Behavior in a Circular-Cylindrical Orifice Flow, *JSME International Journal Series B Fluids and Thermal Engineering*, *45* (2002), 3, pp. 638-645
[17] Zhao, W. G., *et al.*, Numerical Study on the Control Mechanism of Cloud Cavitation by Obstacles, *Journal of Hydrodynamics, Ser. B*, *22* (2010), 5, pp. 792-797
[18] Che, B., *et al.*, Control Effect of Micro Vortex Generators on Attached Cavitation Instability, *Physics of Fluids*, *31* (2019), 6, 064102
[19] Zhang, L., *et al.*, Inhibition of Cloud Cavitation on a Flat Hydrofoil Through the Placement of an Obstacle, *Ocean Engineering*, *155* (2018), May, pp. 1-9
[20] Zhao, G., *et al.*, Towards the Control of Blade Cavitation in a Waterjet Pump with Inlet Guide Vanes: Passive Control by Obstacles, *Ocean Engineering*, *231* (2021), July, 108820
[21] Menter, F. R., Two-Equation Eddy-Viscosity Turbulence Models for Engineering Applications, *AIAA Journal*, *32* (1994), 8, pp. 1598-1605
[22] Bardina, J., *et al.*, Turbulence Modeling Validation, *Proceedings,* 28th Fluid Dynamics Conference, Sowmass, Call., USA, 1997, p. 2121
[23] Simpson, A., Ranade, V. V., Modeling Hydrodynamic Cavitation in Venturi: Influence of Venturi Configuration on Inception and Extent of Cavitation, *AIChE Journal*, *65* (2019), 1, pp. 421-433
[24] Simpson, A., Ranade, V. V., Modelling of Hydrodynamic Cavitation with Orifice: Influence of Different Orifice Designs, *Chemical Engineering Research and Design*, *136* (2018), Aug., pp. 698-711
[25] Rhie, C. M., Chow, W. L., Numerical Study of the Turbulent Flow Past an Airfoil with Trailing Edge Separation, *AIAA Journal*, *21* (1983), 11, pp. 1525-1532
[26] Gillieron, P., Patent, FR 2 848 521 – A1, 2002
[27] Gustavsson, T., Patent, WO-2003045768 A1, 2003

Paper submitted: February 10, 2023
Paper revised: February 28, 2023
Paper accepted: June 10, 2023

© 2023 Society of Thermal Engineers of Serbia.
Published by the Vinča Institute of Nuclear Sciences, Belgrade, Serbia.
This is an open access article distributed under the CC BY-NC-ND 4.0 terms and conditions.